Experiments on Flow-Distributed Oscillations in the Belousov−Zhabotinsky Reaction

Mads Kærn[†] and Michael Menzinger*[,‡]

Center for BioDynamics and Department of Biomedical Engineering, Boston University, 44 Cummington Street, Boston, Massachusetts 02215, and Department of Chemistry, University of Toronto, 80 St. George Street, Toronto, Ontario M5S 3H6, Canada

Received: August 8, 2001; In Final Form: January 18, 2002

This paper presents an overview of the waves and patterns that are formed when the oscillatory Belousov−Zhabotinsky medium flows through a packed bed reactor. At a sufficiently high flow velocity, this flow-distributed oscillation (FDO) gives rise to stationary waves with constant forcing at the inflow and to traveling waves with periodic forcing at the inflow. The wavelength of the stationary FDO wave is found to depend on flow velocity and on the effective diffusion coefficient (diameter of packing medium). We demonstrate the breakdown of stationary FDO waves at low flow velocity at which the space-periodic structure is replaced by irregular waves. At high flow velocity, periodic boundary forcing is found to give FDO waves that propagate either with a constant or with an oscillatory velocity. The wavelength and the velocity of the constant velocity upstream or downstream propagating waves are found to agree quantitatively with those predicted theoretically. Finally, we investigate the effect of a frequency gradient on FDO waves. When the oscillation period of the medium increases with the distance from the reactor inlet, it is observed that waves propagate downstream with a decreasing width and velocity. The behavior of both the waves propagating with an oscillatory velocity and those formed in the presence of a frequency gradient can also be understood in terms of phase dynamics.

1. Introduction

The concept of flow-distributed oscillations (FDO) was introduced[1] to explain the formation of stationary space-periodic structures in boundary-forced open flows of oscillatory media. The existence of these structures was surprising at the time of their theoretical prediction,[2,3] because they arise in the absence of the diffusive or the advective differential transport that is usually required for the breaking of spatial symmetry.[4,5] It turned out that the structures are essentially kinematic in nature and arise from the spatial resolution of the oscillation phase by the flow.[1,6] Because the governing physical mechanism is simple, FDO waves enjoy a great generality and they are not restricted, like many other spatio-temporal structures, to relatively small regions of parameter space.

Since the discovery of FDO waves, several studies have been focused on theoretical issues. Bamforth et al. studied FDO waves theoretically and numerically using models of the chlorine−dioxide−iodide−malonic (CDIMA)[7] and of the Belousov−Zhabotinsky (BZ)[8] reaction. As in the earlier works,[2,3] a flow of oscillatory medium with equal flow and diffusion coefficients was investigated. The results were also similar: FDO waves are generated when an open flow of a medium that oscillates under well-stirred conditions is constantly forced at the inflow boundary, provided that the flow velocity is sufficiently high. By generalizing the mathematical analysis to the case involving differential transport, Satnoianou and Menzinger[9] showed that oscillatory batch-mode kinetics is not always necessary and that stationary structures may also form for parameter values for which the batch-mode kinetics supports only a stable steady state. These generalized patterns, referred to as FDS waves, are observed within the region of parameter space where traveling waves can be induced by the differential flow instability.[9] Finally, FDO-like patterns have also been observed in the models of cross-flow reactors studied by Nekhamkina et al.[10]

In section 2, the present paper gives an introductory theoretical and phenomenological overview of FDO waves. This is followed in sections 3 and 4 by an experimental investigation of the stationary and traveling FDO waves that arise when the oscillatory BZ medium flows through a packed-bed reactor (PBR). The experimental setup is described in section 3. The investigation of stationary FDO waves formed when the inflow boundary is constantly forced is presented in section 4.1. It was observed that the wavelength, λ, of the FDO waves increases more or less linearly with the flow velocity and that increasing the effective diffusion coefficient, which depends on the size of the PBR packing material, decreases the wavelength. Model analysis suggests that the stationary FDO waves cease to exist when the flow velocity is decreased below a critical value.[2,3,7−10] At intermediate flow velocities, we observed a competition between a stationary FDO and an irregular structure. The irregular structure became dominant when the flow velocity was decreased further. We believe that irregular waves may be an example of a noise-sustained structure.[11] Such structures are expected in the region of parameter space where the system has a convectively unstable homogeneous state.[11] Consistent with the hypothesis, Bamforth et al.[8] predicted, using the Oregonator model of the BZ system, that a transition from space-periodic FDO waves to a convectively unstable homogeneous state takes place when the flow velocity is decreased.

The investigation of traveling FDO waves formed when the inflow of the PBR is periodically forced is presented in section 4.2. Depending on the kinetic conditions at the inflow boundary, upstream or downstream waves with constant or oscillatory velocity waves are observed. The wavelength and the velocity

* To whom correspondence should be addressed. E-mail: mmenzing@chem.utoronto.ca. Fax: 416-978-6158.
[†] Boston University.
[‡] University of Toronto.

10.1021/jp013095f CCC: $22.00
Published on Web 04/20/2002

of the constant velocity waves were found to be in quantitative agreement with the theoretical predictions. We also investigated the effect of imposing a temperature gradient along the flow reactor such that the oscillation period of the downstream moving medium increases with the distance from the reactor inlet. The result is FDO waves that propagate downstream with decreasing width and velocity. Such waves have been argued to be involved in biological pattern formation.[12]

2. Theoretical Section

The experimental system described in section 3 can, to a first approximation, be described as a transversely uniform, ideal plug-flow reactor in which all species have equal flow and diffusion coefficients. It is described mathematically by the reaction−diffusion−advection equation:

$$\frac{\partial \mathbf{u}}{\partial t} = \mathbf{f}(\mathbf{u}) + D\frac{\partial^2 \mathbf{u}}{\partial x^2} - \phi\frac{\partial \mathbf{u}}{\partial x'} \tag{1}$$

where x is the spatial coordinate, $0 \le x \le L$, $\mathbf{u}$ is a vector of chemical concentrations, and D and ϕ are the diffusion and flow coefficients, respectively. The boundary conditions are no-flux at the outflow, $x = L$, and $\mathbf{u}(t,x{=}0) = \mathbf{u}_t(t)$ at the inflow. The initial condition, $\mathbf{u}(t{=}0, 0{<}x{<}L)$ is not important when the system is convectively unstable, because the mode that arises from the initial *condition* is eventually washed out of the system. In the following, it is assumed that eq 1 oscillates with period T_0 in the absence of flow and diffusion (i.e., under well-stirred batch-mode conditions).

Equation 1 can be made dimensionless by defining new space and time coordinates, τ and y, given by $\tau = t/T_0$ and $y = x/(\phi T_0)$. The result is the dimensionless equation

$$\frac{\partial \mathbf{u}}{\partial \tau} = T_0\mathbf{f}(\mathbf{u}) + \frac{D}{\phi^2 T_0}\frac{\partial^2 \mathbf{u}}{\partial y^2} - \frac{\partial \mathbf{u}}{\partial y} \tag{2}$$

In the reference frame $z = y - \tau$ that moves with the flow, the local dynamics is determined by

$$\frac{\partial \mathbf{u}}{\partial \tau} = T_0\mathbf{f}(\mathbf{u}) + \epsilon\frac{\partial^2 \mathbf{u}}{\partial z^2} \tag{3}$$

where the dimensionless parameter ϵ is defined by the ratio $\epsilon = D/(\phi^2 T_0)$. It measures the relative strength of advection and diffusion. The limit $\epsilon \to 0$ corresponds to negligible diffusion and is referred to as the kinematic limit. With the exception of the changed time scale, $t = \tau T_0$, the dynamics in the moving reference frame (eq 3) coincides with that of the well-stirred batch-mode system (eq 1 with D and ϕ equal to zero). In other words, in the kinematic limit, volume elements behave as tiny batch reactors and oscillate with period T_0 as they are carried downstream.

Most of the theoretical investigations mentioned in the Introduction[2,3,7−10] focus on the transition between the two domains of parameter space where the dynamics is dominated by reaction−diffusion ($\epsilon \gg 1$) and by reaction−advection, ($\epsilon \ll 1$). Here, we investigate the latter region using phase dynamics. The use of phase dynamics does not require that diffusion is negligible, and it is not necessary to assume the kinematic limit. Because eq 3 is known to oscillate when ϵ is zero, it is, for reasons of continuity, reasonable to assume that it also has a periodic solution for small values of ϵ. In other words, there exists some range of finite ϵ values below a critical value ϵ_c in which volume elements oscillate with a period T that is different from the batch-mode oscillation period T_0 (unity in eq 3). This corresponds to a sufficiently high flow velocity, $\phi > \phi_c$. It is this oscillation that defines the FDO and the region of parameter space where $\epsilon < \epsilon_c$ (or $\phi > \phi_c$) defines the region where FDO waves are observed. The period $T(D,\phi,T_0)$ of the FDO is referred to in the following as the *intrinsic period*.

TABLE 1: The FDO Waves Predicted for Different Ratios $R = T'/T$ of the Forcing Period T' and the Intrinsic Period T

ratio	velocity	wave type
$R = \infty$	$c = 0$	stationary
$R > 1$	$c > 0$	upstream traveling
$R = 1$	$c = \infty$	homogenous oscillation
$R < 1$	$c < 0$	downstream traveling

A volume element injected at $x = 0$ at time t_0 has been carried at time t the distance given by $x = (t - t_0)\phi$ in the downstream direction. Meanwhile, its oscillation phase, θ, has advanced from its initial value by $\Delta\theta = (t - t_0)/T$. If the volume element has entered the flow with the initial phase $\theta_0(t_0) = t_0/T'$, where T' is the forcing period at the boundary ($T' = \infty$ corresponds to constant forcing), it has at time t and distance x a phase value that is given by

$$\theta(x,t) = \theta_0(t_0) + \frac{t - t_0}{T} = \frac{x}{\phi}\left(\frac{1}{T} - \frac{1}{T'}\right) + \frac{t}{T'} \tag{4}$$

This phase function can be used to calculate both the phase velocity c and the wavelength λ of the FDO waves.[12] The velocity is derived from the fact that the phase is an exact differential of space and time. It is obtained by setting $\mathrm{d}\theta(x,t) = \partial_t\theta\ \mathrm{d}t + \partial_x\theta\ \mathrm{d}x$ equal to zero as

$$c = \frac{-\phi}{R - 1} \tag{5}$$

where the partial derivatives are obtained from eq 4 and R is defined as the ratio of the periods at the boundary and in the reactor, $R = T'/T$. As summarized in Table 1, phase dynamics predicts four principal wave-types with different phase velocities. For $R = \infty$ (constant boundary forcing), it predicts a stationary wave ($c = 0$). For $R > 1$, $R = 1$, and $R < 1$, it predicts an upstream propagating wave ($c < 0$), a homogeneous wave with infinite velocity ($c = \infty$), and a downstream propagating wave ($c > 0$). Note that the derivation of the phase function in eq 4 is based on the implicit assumption that the initial phase θ_0 increases linearly with time. The breakdown of this assumption has a significant effect on the spatio-temporal wave behavior and gives rise to the "jumping waves" discussed in section 4.2.

The wavelength of the FDO waves can also be obtained from the phase function. It is the distance between locations having a phase difference of one. It is obtained from the relation $|\theta(x,t) - \theta(x\pm\lambda,t) = 1|$ as

$$\lambda = \frac{\phi T'}{|R - 1|} \tag{6}$$

For constant boundary forcing ($T' = \infty$), for which eq 5 predicts a stationary wave, $c = 0$, rearrangement of eq 6 gives a relationship between the wavelength of the FDO wave, the flow velocity ϕ, and the intrinsic oscillation period T. It is in general form given by

$$\lambda = \phi T(D,\phi,T_0) \tag{7}$$

In the kinematic limit, in which the intrinsic period is constant and equal to the batch-mode oscillation period, $T = T_0$, the wavelength is a linear function of the flow velocity.[1] Away from

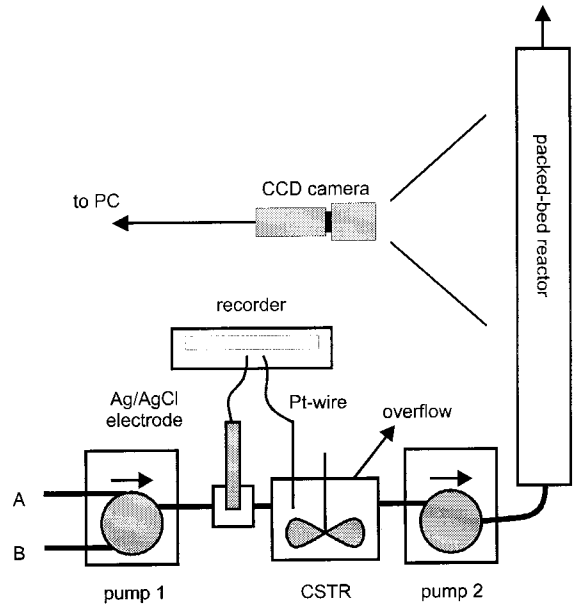

Figure 1. Experimental setup. A peristaltic pump (labeled 1) feeds the continuously stirred tank reactor (CSTR) at a constant rate. It is monitored by a Pt-electrode and a double-junction Ag/AgCl electrode placed in the feed stream prior to the CSTR. Reaction mixture is removed from the CSTR through the vertical packed-bed reactor and through an overflow drain. The second peristaltic pump (labeled 2) controls the flow through the packed-bed reactor(s).

this limit, the intrinsic period T (and hence the wavelength) depends on the details of the system and it may be either shorter[1,13] ($T < T_0$), unchanged[7] ($T = T_0$), or longer[14] ($T > T_0$) than that predicted for the purely kinematic wave.

FDO waves bear witness to the fact that the spatio-temporal behavior of convectively unstable open flows is determined by the temporal dynamics at the inflow boundary.[11] The organization occurs as the forcing frequency is imposed onto the entire system. This can be seen directly from the phase function, eq 4. Differentiation of $\theta(x,t)$ with respect to time shows that each point in space oscillates with the forcing period, $\partial\theta/\partial t = 1/T'$. Hence, the periods of the intrinsic as well as the forcing oscillation can be obtained directly from a space-time plot of the oscillation phase $\theta(x,t)$; T' can be measured as the temporal recurrence of oscillation phase at any fixed spatial locations, while T can be measured along lines $x = \phi(t - t_0)$ that follow the location of individual volume elements.

3. Experimental Section

The experimental setup is illustrated in Figure 1. In the basic configuration, it comprises a single vertically mounted glass tube packed with glass beads, a PBR, which is fed BZ reaction medium from a continuously stirred tank reactor (CSTR). The peristaltic pump labeled 2 controls the velocity with which volume elements are carried through the PBR. The CSTR was fed stock solutions (A = malonic acid and ferroin, B = bromate and sulfuric acid) at a rate controlled by the pump labeled 1. The setting of pump 1 was always higher than that of pump 2 and excess reaction medium was removed through the CSTR overflow port. A typical composition after mixing was $[H_2SO_4] = 0.15$ M, $[BrO_3^-] = 0.2$ M, [malonic acid] = 0.4 M, [ferroin] $= 7.5 \times 10^{-4}$ M.

The residence time of the CSTR, which is controlled by pump 1, is an important control parameter because it determines the (forcing) state at the reactor inlet. The CSTR is in an oscillatory state when the residence time is long and in a steady state when the residence time is short.[1,15] Hence, constant and periodic boundary forcing can be achieved with the same experimental setup by changing the setting of pump 1 without changing the flow through the PBR. Furthermore, changing the setting of pump 1 allowed for some control of the ratio R of the forcing period T' to the intrinsic oscillation period T when the CSTR was in the oscillatory state. The experiments presented in section 4 were carried out using a number of slightly different experimental conditions to get a broad range of R values. In experiments that used the configuration shown in Figure 1, the CSTR oscillation period T' was longer than the batch-mode period T_0 and the intrinsic period T, that is, $R > 1$. To achieve a forcing period that is shorter than the batch-mode oscillation period, $R < 1$, the CSTR in Figure 1 was fed reaction mixture using three feedstreams containing malonic acid, ferroin, and acidified bromate. The two latter feeds were mixed in a second 0.5 mL CSTR before being fed to the CSTR shown in Figure 1. This premixing caused the reagent mixture to be in the excited state. The forcing period was further manipulated by adding sodium bromide (micromolar range) to the stock solution containing either malonic acid or ferroin. Finally, we did experiments using different concentrations of ferroin, (10^{-4}−10^{-3} M range), malonic acid (0.05−0.4 M range), and bromate (0.05−0.4 M range) in the CSTR feedstreams to ensure that the formation of phase waves is indeed robust. While the CSTR oscillation period was measured in all of the experiments, we did not investigate systematically how the forcing and the batch-mode oscillation periods change in the various configurations and with the various feed-stream concentrations.

The flow reactor was illuminated from the back by two fluorescent tubes and the transmittance was recorded using a black-and-white charged-coupled device (CCD) camera equipped with a 450−550 nm band-pass filter. The red reduced ferroin complex absorbs strongly at these wavelengths, while the blue oxidized ferriin complex does not. Hence, the transmittance through the flow reactor depends on the relative concentration of ferriin. The oscillation phase in which the concentration of ferriin is high appears white on a black background. Snapshots of the flow reactor were transferred directly to a personal computer using commercially available hardware and software (DataTranslation DT3155 frame-grabber, HLImage). The pixel intensity maps were extracted as 8-bit gray scale portable pixel maps and analyzed using custom-written programs.

The purpose of the glass beads is to induce turbulent mixing within the packed bed and to ensure that the flow profile is uniform and perpendicular to the pressure gradient. This is important to maintain lateral phase coherence within the reactor. In addition, the turbulent mixing has the effect of increasing the effective diffusion coefficients to values that are typically orders of magnitude greater than those of molecular diffusion. At the flow velocity employed in the present experiments, all species can be assumed to have the same effective diffusion coefficient. It is approximately given by $D = d_p\phi$, where d_p is the diameter of the packing material.[16,17] The linear flow velocity was estimated either by measuring the volumetric flow rate and the void space of the packed bed or by measuring the velocity of the gas/liquid interface when the reactor was initially filled.

4. Results

4.1. Constant Boundary Forcing. Representative examples of stationary waves observed with constant boundary forcing are shown in Figure 2. The three panels are space−time plots obtained by stacking successive images of a PBR packed with 1 mm beads with time progressing from left to right. The inflow

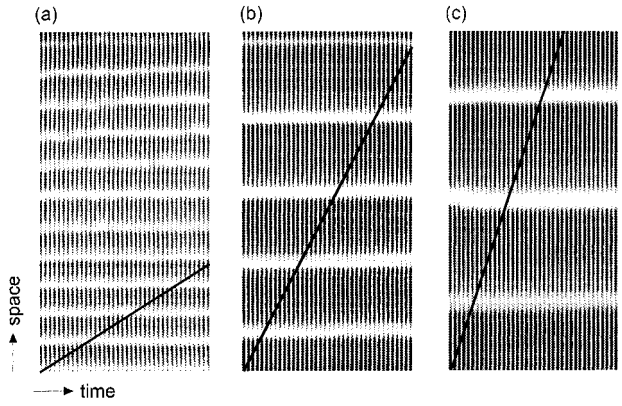

Figure 2. Stationary FDO waves at different flow velocities. The space−time plot is obtained by stacking successive snapshots taken at a rate of four per minute. Time progresses from left to right. Each snapshot shows 64 cm of the PBR. The solid line gives the location of a volume element as it is carried downstream (upward). Flow velocities are (a) 0.04, (b) 0.11, and (c) 0.17 cm/s.

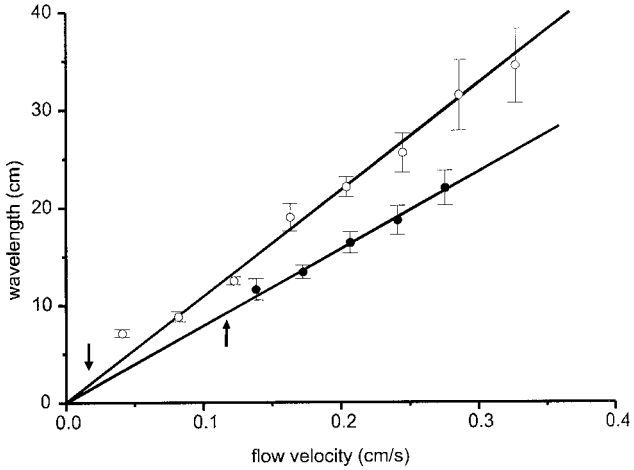

Figure 3. The dependence of the wavelength on the flow velocity for 3 mm (●) and 1 mm (○) diameter glass beads. The arrows indicate the approximate location of the critical flow velocity.

is at the bottom and the slanted line shows the location of a volume element as it is carried downstream by the flow. The intrinsic oscillation period $T(D,\phi,T_0)$ can be readily read off this line. It is about 2 min (8 frames) in Figure 2c and slightly longer (9−10 frames) in Figure 2a,b. To investigate the dependence of the wavelength on the flow velocity and on the size of glass beads (i.e., on the turbulent diffusion coefficient; see above), flow-reactors packed with $d_p = 1$ and $d_p = 3$ mm beads were connected simultaneously to the CSTR. This ensures that the waves in the two reactors are directly comparable. The result of this experiment is summarized in Figure 3, which shows the wavelengths measured at different flow velocities. The wavelength is observed to be fairly linear for both 1 mm (open circles) and 3 mm beads (filled circles), at least at high flow velocities. When the flow velocity is below 0.14 cm/s, irregular traveling rather than stationary waves were observed in the reactor with 3 mm beads. In the reactor with 1 mm beads, the stationary FDO waves were replaced by irregular waves (see also Figure 4) when the flow velocity is less than about 0.03 cm/s. This critical flow velocity agrees well with the value of $\phi_c = 0.01$ cm/s predicted by linear stability analysis using molecular diffusion in the Oregonator model.[8]

The relaxation time of the stationary FDO waves is quite long at low flow velocities. Sometimes (see Figure 4), it was observed that the stationary wave breaks down and then, over time,

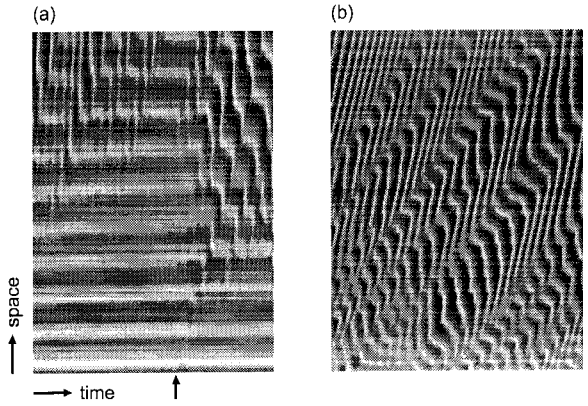

Figure 4. Wave behaviors at low flow velocity. Space−time plots of the averaged transmittance at (a) $\phi = 0.03$ cm/s and (b) $\phi = 0.01$ cm/s are shown. The stationary FDO wave competes with an irregular structure in panel a and fails to establish in panel b. The length and time scales of both plots are 34 cm and 53 min. The experimental conditions are the same as in Figure 2 except that the concentration of malonic acid is 0.2 M.

reestablishes itself. The long relaxation time poses a major challenge to the quality of the measurements because CO_2 released by the medium is trapped within the reactor and the actual flow velocity therefore increases with time. In a PBR with a free volume of 10 cm^3, the volume occupied by CO_2 was measured to be 2.7 cm^3 (27%) after 2 h at $\phi = 0.01$ cm/s (1 mm beads). The uncertainty in the linear flow velocity in Figure 3 is thus quite large, and the dependence of the wavelength and intrinsic oscillation period on the parameter is not available in quantitative detail. It is nevertheless clear from Figure 3 that the wavelength at a given flow velocity is significantly decreased when the bead size is increased. This observation can be understood in terms of turbulent diffusion within the packed bed and the properties of the BZ reaction medium. Because increased bead size causes the effective diffusion coefficient to increase (see section 3), the effect of increased bead size should be qualitatively similar to increasing the diffusion coefficient. The spatial profiles (not shown) of the stationary FDO waves have a sharp, narrow autocatalytic front followed by a smooth and broad refractory tail. A wave train of this type generally has a wavelength that decreases when the diffusion coefficient is increased as the autocatalytic front can penetrate deeper into the refractory tail.[1]

As described in section 2, FDO waves are formed when the flow velocity is above a certain critical value, ϕ_c. Figure 4 shows the wave behavior at low flow velocities, $\phi = 0.03$ cm/s in panel a and $\phi = 0.01$ cm/s in panel b, in a reactor packed with $d_p = 1$ mm beads. In Figure 4a, there is a competition between irregular traveling waves and stationary FDO waves. A stationary wave is initially established, but it breaks down into irregular traveling waves. The breakdown of the stationary wave appears to be caused by a perturbation at the boundary (indicated by the arrow) that spreads in the downstream direction. The effect of decreasing the flow velocity further is shown in Figure 4b. No stationary waves can be observed, and the irregular waves now fill the entire reactor. Hence, the irregular waves are favored when the flow velocity is decreased. As it will be discussed in section 5, the irregular wave structure may be a noise-sustained structure generated when the system supports a convectively unstable homogeneous state.

4.2. Periodic Boundary Forcing. Periodic boundary forcing can be achieved by increasing the CSTR residence time above a critical value. The experiments with periodic forcing involved a PBR packed with $d_p = 1$ mm glass beads. With the CSTR

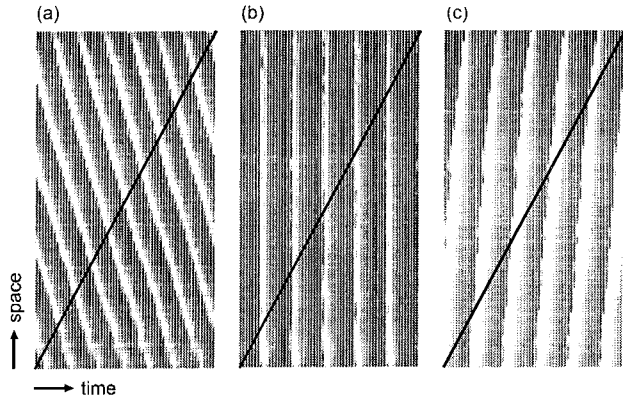

Figure 5. Traveling FDO waves. Upstream traveling waves (a), homogeneous oscillation (b), and downstream traveling waves (c) were observed with different ratios of intrinsic and forcing periods at $\phi = 0.10$ cm/s. Sixty-one frames, taken at intervals of 10 s and showing 63 cm of the flow-reactor, are displayed in each panel.

feed-stream concentrations listed in section 4.1, the intrinsic oscillation period T is shorter than the batch-mode oscillation period T_0. Hence, the ratio $R = T'/T$ was, in the typical experiment, less than one, and upstream propagating waves were the most frequently observed wave type. The case of $R > 1$ was achieved by changing the CSTR feed-stream concentrations, for instance, by premixing and exciting the feed streams using a second CSTR with a very short residence time, by changing the CSTR residence time, or by changing the CSTR feed-stream concentrations, as it was described in section 3.

Figure 5 shows representative examples of (a) upstream propagating waves, (b) homogeneous oscillations, and (c) downstream propagating waves. The number of displayed frames corresponds to the time that it takes a volume element that is injected into the flow reactor at the lower left corner to be carried across the entire length of the reactor. This volume element moves along the diagonal line shown in each of the three panels. Note that the intrinsic oscillation period is different in the three panels. This is due to the different feed-stream compositions used in each experiment. In agreement with the predictions in section 2, there is temporal recurrence with period T' of the oscillation phase at each fixed point x within the flow reactor. In all cases, it was found to coincide with the period of the CSTR measured potentiometrically. The effect of CO_2 accumulation was minimized by carefully removing accumulated CO_2 between experiments and by using relatively high flow velocities.

Because the experiments involve different flow velocities and different compositions of the medium, it is necessary to express the equations for the wavelength and the wave velocity in a form that is independent of the actual parameter values. Suitable dimensionless forms of eqs 5 and 6 are given by

$$\frac{\phi}{c} = 1 - R, \quad \frac{\phi T'}{\lambda} = |R - 1| \tag{8}$$

respectively. Figure 6 compares the relationship between the measured values of T', T, c, and λ to those predicted by phase dynamics (eq 8, drawn with full and dashed lines). The agreement between the measured and the predicted relationships is quantitative. This confirms the validity of eqs 5 and 6 and of the hypothesis that the waves are phase waves.

An intriguing change in spatio-temporal dynamics is observed when the CSTR residence time is decreased from the relatively high values used in Figure 6 and approaches the value at which the CSTR changes from oscillatory to stationary. This change

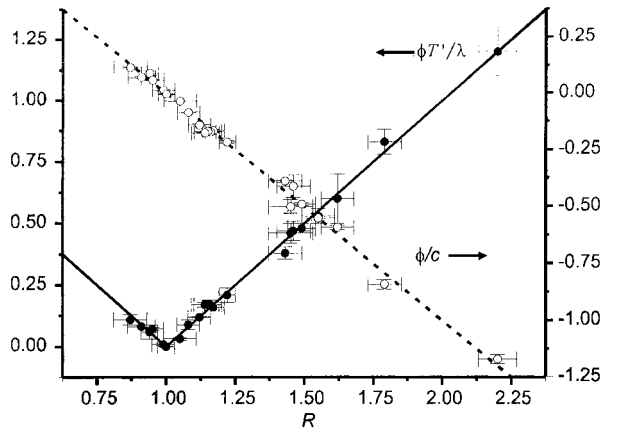

Figure 6. Quantitative agreement between the theoretically predicted relationships among c, ϕ, T, and T' (full and dashed lines) and those measured experimentally (circles).

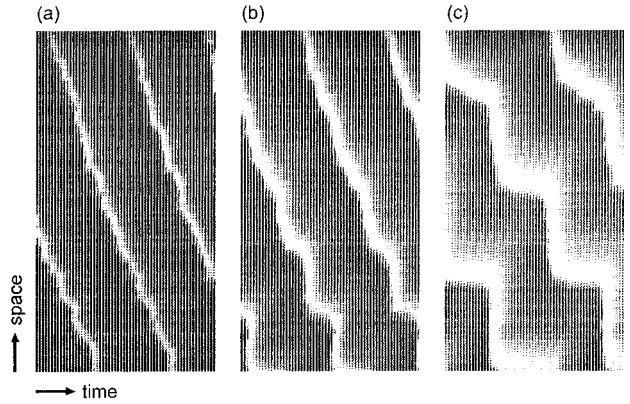

Figure 7. Effects of decreased CSTR residence time: (a) a smooth downstream traveling wave at long residence time (low k_0). The residence time is half (k_0 doubled) in panel b and the wave has an oscillatory velocity close to the reactor inlet. In panel c, the CSTR is close to criticality and the oscillation in the wave velocity is particularly pronounced.

is illustrated in Figure 7. In the experiments, the CSTR output was directly connected to the flow reactor inlet, and a decreased residence time gave rise to an increased flow velocity in the flow reactor. With this feeding configuration, the decreased CSTR residence time caused the period of the forcing oscillation to increase. This is primarily the result of a longer refractory phase of the relaxation oscillation.[6]

Figure 7a illustrates waves that propagate upstream with a rather constant velocity, given the flow rate of $\phi = 0.037$ cm/s. In Figure 7b, the flow velocity was increased to $\phi = 0.075$ cm/s and the CSTR residence time is decreased by a factor of 2. Close to the reactor inlet, the waves propagate with an oscillatory velocity and a phase of slow propagation alternates with a phase of rapid propagation. This intriguing behavior becomes more pronounced in Figure 7c when the flow velocity is further increased to $\phi = 0.112$ cm/s. The space−time plot now has the shape of a staircase. The waves remain stationary for a certain time, and then suddenly jump to a new upstream location where they again become stationary. This behavior is not transient, and it persists over an extended time. Note that the volume elements carried downstream still oscillate with a nearly constant period and that a given oscillation phase recurs periodically at any fixed spatial point. Thus, the jumping waves are phase waves that are controlled by the boundary forcing.

The oscillatory wave velocity is a kinematic effect that arises as the result of different kinetic conditions in the CSTR and in

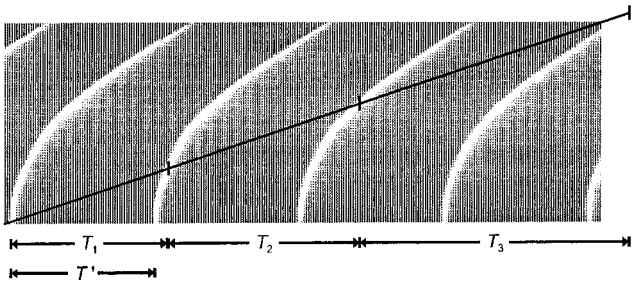

Figure 8. FDO waves observed when the intrinsic period decreases with the distance to the inflow boundary (see text).

the flow reactor.[6] Increasing the residence time in the CSTR lengthens the refractory phase of the forcing oscillation. During this phase the concentrations change relatively slowly and the elongation of the refractory tail corresponds essentially to an interval of constant boundary forcing. On the other hand, the excited phase of the relaxation oscillation is more or less unaffected by the increased residence time. As a result, the boundary forcing does not correspond to a linearly increasing initial phase value as it was assumed in section 2. Instead, the PBR experiences a constant force during the time interval when the CSTR is in the slowed-down refractory phase and the value of R oscillates between a value of zero (stationary FDO) and one (homogeneous oscillation). The result is a staircase-shaped space−time plot.

Finally, we investigated the effect of having a gradually increasing the intrinsic oscillation period $T(x)$ as medium is carried downstream. It was achieved by imposing a temperature gradient along the flow tube by heating the CSTR and the inlet of the PBR to 45 °C, while allowing for the free cooling of its downstream upper part. The experiments were done with a large CSTR to obtain relatively long residence times and an oscillation period and profile close to those of the batch-mode oscillation. The CSTR was a 300 mL Erlenmeyer flask and had a residence time of approximately 15−20 min. The flask was immersed into a heated water bath that was placed on top of a magnetic stirrer. The CSTR was open to air to allow escape of gases released from the heated BZ medium. An example of FDO waves observed under these conditions is shown in Figure 8. It displays 256 frames showing 61 cm of the reactor and taken at 1-s intervals.

The effect of the downstream decreasing temperature is to increase the intrinsic oscillation period $T(x)$ as volume elements are carried downstream ($\phi = 0.24$ cm/s) The slanted line in Figure 8 shows the approximate location of such a volume element and the steadily increasing oscillation period $T_1 < T_2 < T_3$ given by the distance between the ticks on this line. As a result, the value of R decreases with increasing distance from the inflow boundary. This generates phase waves that propagate downstream with decreasing velocity and wavelength. Note that it can be quite difficult to maintain a constant oscillation period and profile in the CSTR and the homogeneous oscillation near the inflow boundary, shown in Figure 8, could only be maintained over a short period of time. In other experiments (not shown), the phase wave appeared at a short distance downstream from the inflow and split into an upstream and a downstream traveling component.

5. Discussion

We have presented an overview of the various spatio-temporal waves and patterns that arise when an open flow of an oscillatory medium is subjected to constant or periodic forcing at the inflow boundary. Constant forcing gives rise to stationary waves, while periodic forcing gives rise to traveling waves. At high flow rates, the velocity and wavelength of the waves are in perfect agreement with kinematic wave theory, which proves that they are indeed phase waves generated by the flow-distributed batch-mode oscillation. Diffusion plays only a secondary role and is not a required component of the pattern-forming mechanism. Diffusion, however, plays an important role in determining the wavelength of the structure. We observed that there is a dramatic decrease in the wavelength of the stationary FDO waves when the effective diffusion coefficient within the packed bed is increased.

At sufficiently low flow velocity, the stationary FDO waves were replaced by irregular wave structures. The critical flow velocity at which their breakdown occurs is lowered when the effective diffusion coefficient is decreased. In agreement with theoretical predictions, this indicates that a sufficiently low ratio of diffusive to advective transport coefficient is required for the formation of FDO waves. Theoretical work has shown that FDO waves can only arise in the region of parameter space where the system is convectively unstable.[2,3,7−9] In open flows in general, advection converts a temporal periodicity (period T') into a spatial periodicity (wavelength $\phi T'$).[18] Convectively unstable flows have the special property that the boundary forcing can organize the entire system spatially and temporally by amplification of the modes imposed at the boundary. This organization is common to all convectively unstable flows and is not restricted to open flows of oscillatory media.[18] However, the FDO phenomenon is a perfect example of such local control of global dynamics.

Convectively unstable open flows act as noise amplifiers and are usually associated with the formation of noise-sustained structures. When linear stability analysis predicts a convectively unstable homogeneous state, this state cannot be expected in an experimental setting because even low-amplitude boundary fluctuations are amplified spatially.[11] This has, for instance, been demonstrated for the case of the differential flow instability[19,20] in which noise breaks the spatial symmetry of the convectively unstable homogeneous state and gives rise to traveling waves. An interesting question that remains to be solved is the competition between structures imposed onto the system by boundary forcing and structures sustained by noise. FDO waves and noise-sustained Hopf structures arise in the same region of parameter space (convectively unstable conditions, batch-mode oscillation, and equal flow and diffusion coefficients) in the absence and presence of boundary noise, respectively. Similarly, for the case of differential flows, FDS and DIFI waves are formed more or less in the same region of parameter space but in the absence and presence of boundary noise, respectively. The irregular structure that replaces the stationary FDO wave at low flow velocity (Figure 4) may be an example of a competition between FDO waves and noise-sustained Hopf structures near the bifurcation from space-periodic structures to a convectively unstable homogeneous state predicted theoretically.[8] The spatio-temporal behavior in Figure 4b also looks similar to noise-sustained Hopf structures observed in numerical simulations.[14] However, whether and when noise-sustained structures replace FDO waves and when traveling DIFI waves replace stationary FDS waves need verification by future theoretical and experimental investigations.

Acknowledgment. We thank R. Satnoianou, S. Kalliadasis, and J. H. Merkin for useful discussions related to this work. M.K. was supported by a Fellowship from the Danish Research Academy. Operating grant was provided by NSERC.

References and Notes

(1) Kærn, M.; Menzinger, M. *Phys. Rev. E* **1999**, *60*, 3471.
(2) Kuznetsov, S. P.; Mosekilde, E.; Dewel, G.; Borckmans, P. *J. Chem. Phys*. **1997**, *106*, 7609.
(3) Andrésen, P.; Bache, M.; Mosekilde, E.; Dewel, G.; Borckmans, P. *Phys. Rev. E* **1999**, *60*, 297.
(4) Turing, A. M. *Philos. Trans. R. Soc. London, Ser. B.* **1952**, *237*, 37.
(5) Rovinsky, A. B.; Menzinger, M. *Phys. Rev. Lett.* **1993**, *70*, 778.
(6) Kærn, M.; Menzinger, M. *Phys. Rev. E* **2000**, *61*, 3335; *Phys. Rev. E* **2000**, *62*, 2994.
(7) Bamforth, J. R.; Kalliadasis, S.; Merkin, J. H.; Scott, S. K. *Phys. Chem. Chem. Phys.* **2000**, *2*, 4013.
(8) Bamforth, J. R.; Merkin, J. H.; Scott, S. K.; Toth, R.; Gaspar, V. *Phys. Chem. Chem. Phys.* **2001**, *3*, 1435.
(9) Satnoianu, R.; Menzinger, M. *Phys. Rev. E* **2000**, *62*, 113.
(10) Nekhamkina, O. A.; Nepomnyashchy, A. A.; Rubinstein, B. Y.; Sheintuch, M. *Phys. Rev. E* **2000**, *61*, 2436.
(11) Deissler, R. J. *J. Stat. Phys.* **1985**, *40*, 371; *J. Stat. Phys.* **1989**, *54*, 1459.
(12) Kærn, M.; Menzinger, M.; Hunding, A. *Biophys. Chem.* **2000**, *87*, 121; *J. Theor. Biol.* **2000**, *207*, 473.
(13) Andrésen, P.; Mosekilde, E.; Dewel, G.; Borckmans, P. *Phys. Rev. E* **2000**, *62*, 2992.
(14) Kærn, M. On the spatio-temporal dynamics of boundary forced open reactive flows. Ph.D. Thesis, University of Toronto, Toronto, Canada, 2001.
(15) Schmitz, R. A.; Graziani, K. R.; Hudson, I. L. *J. Chem. Phys.* **1977**, *67*, 3040.
(16) Wakao, N.; Kaguei, S. *Heat and mass transfer in packed beds*; Gordon and Breach Science Publishers: New York, 1982.
(17) Froment, G. F.; Bischoff, K. B. *Chemical reactor analysis and design*; Wiley: New York, 1990.
(18) Kærn, M.; Menzinger, M.; Satnoianu, R.; Hunding, A. *Faraday Discuss.*, in press.
(19) Wu, X. G.; Nakata, S.; Menzinger, M.; Rovinsky, A. B. *J. Phys. Chem.* **1996**, *100*, 15810.
(20) Satnoianu, R.; Merkin, J. H.; Scott, S. K. *Dyn. Syst. Appl.* **1999**, *14*, 275.